Journal of Alloys and Compounds 506 (2010) 205–209

Contents lists available at ScienceDirect

Journal of Alloys and Compounds

journal homepage: www.elsevier.com/locate/jallcom

Synthesis characterization and magnetic properties of Cr-substituted NiCuZn nanocrystalline ferrite

W.A. Bayoumy [a], M.A. Gabal [b,*]

[a] Chemistry Department, Faculty of Science, Benha University, Benha, Egypt
[b] Chemistry Department, Faculty of Science, King Abdul Aziz University, Jeddah, Saudi Arabia

ARTICLE INFO

Article history:
Received 16 February 2010
Received in revised form 22 June 2010
Accepted 30 June 2010
Available online 3 August 2010

Keywords:
NiCuZn ferrite
Cr substitution
Egg-white
FT-IR
Magnetic properties

ABSTRACT

Egg-white method was used to produce nanocrystalline Cr-substituted NiCuZn ferrites; $Ni_{0.50}Cu_{0.25}Zn_{0.25}Fe_{2-x}Cr_xO_4$ $(0.0 \le x \le 1.0)$ from stoichiometric mixture of their respective metal nitrate. The structural, morphological and magnetic properties of the products were determined by X-ray powder diffractometry (XRD), Fourier transform infrared spectroscopy (FT-IR), transmission electron microscopy (TEM) and vibrating sample magnetometer (VSM). The average crystallite sizes obtained from XRD were between 15 and 25 nm. Magnetization measurements indicated that when the Cr substitution increases the saturation magnetization decreases due to the magnetic character of the chromium ions which prefers octahedral site occupation. The coercivity was found to change proportionally with the particle sizes of the investigated ferrites.

1. Introduction

Ferrites are superior magnetic materials widely used in microwave and electrical industries. They exhibit high electrical resistivity combined with useful ferromagnetic behavior [1]. Low-temperature-fired NiCuZn ferrites have been widely used in inductive multilayer devices because of their relatively high resistivity and good magnetic properties in the high frequency range [2]. Previous investigations of these ferrites mainly focused on how to lower the sintering temperature [3], how to improve electromagnetic properties such as the resistivity, permeability and Q-factor [4] and the co-fired characteristics with an Ag electrode or other ceramics [5].

In recent years, nanocrystalline ferrites have attracted much interest because of their unusual magnetic properties and their promising technological applications. The bulk properties of ferrites changes as its dimensions are changed to nanoscale. The properties of ferrite nanoparticles are influenced by the composition and microstructure, which are sensitive to the preparation methodology used in their synthesis. There are several different synthesis methods used to generate ferrites as reported in the literature including sol–gel [6], coprecipitation [7], hydrothermal [8], mechano-chemical [9], refluxing [10], precursor [11] and auto-combustion [12] methods.

Many efforts have been made to improve the basic properties of NiCuZn ferrite materials by substituting or adding various ions of different valence states depending on the applications of interest.

Nano-sized ferrites of compositions ($Ni_{0.6}Cu_{0.20}Zn_{0.20}Fe_{2-x}Cr_xO_4$), where $x = 0$–1.0, were synthesized through nitrate–citrate auto-combustion method [13]. The system was characterized using XRD, FT-IR and Mössbauer spectroscopy techniques. The electrical properties measurements revealed that, the chromium substitution is decreasing the conductivity and increasing conduction activation energy.

Gabal et al. [14] studied the effect of gallium substitution on the structural, magnetic and electrical properties of $Ni_{0.5}Cu_{0.25}Zn_{0.25}Fe_{2-x}Ga_xO_4$ $(x = 0$–$1.0)$ synthesized using urea combustion method. XRD showed cubic spinel ferrite with an average crystallite sizes in the range of 40–54 nm. Mössbauer measurements indicated that the Ga^{3+} ion prefer to substitute Fe^{3+} ions located in the octahedral site. The measured electrical properties was found to be dependent on the Ga concentration.

Nanocrystalline Mg-substituted NiCuZn ferrites were synthesized using metal nitrates and freshly extracted egg-white [15]. XRD revealed no noticeable variation in the lattice parameters with increasing magnesium content. The saturation magnetization (M_s) and coercivity (H_c) as a function of Mg content were investigated using VSM. It was found that the M_s increases firstly up to $x = 0.2$ and then decreases, while

* Corresponding author. Permanent address: Chemistry Department, Faculty of Science, Benha University, Benha, Egypt. Tel.: +966 557071572.
E-mail address: mgabalabdonada@yahoo.com (M.A. Gabal).

0925-8388/$ – see front matter © 2010 Elsevier B.V. All rights reserved.
doi:10.1016/j.jallcom.2010.06.178

H_c continuously decreases. Magnetic susceptibility measurements give results which agreed well with those obtained by VSM.

Low Mn-doped NiCuZn ferrites with compositions of $(Ni_{0.6}Zn_{0.3}Cu_{0.1})_{1-x}Mn_xFe_2O_4$ (where $x = 0$–0.03) were synthesized using sol–gel method [16]. The influence of the Mn^{2+} content on the microstructure and the magnetic properties was discussed. The saturation magnetization was found to decrease with increasing Mn^{2+} content. The saturation magnetic flux density and remnant magnetic flux density were found to decrease with the Mn^{2+} content up to $x = 0.02$, followed by increasing.

$Ni_{0.25}Cu_{0.2}Zn_{0.55}Sm_xFe_{2-x}O_4$ ferrite with $x = 0.00$–0.075 was synthesized through the nitrate–citrate auto-combustion method [17]. The effect of Sm substitution on phase composition, microstructure and relative density was studied. The permeability, saturation magnetization and AC resistivity were found to increase with Sm substitution up to $x = 0.05$ while magnetic loss decreased.

In previous works, magnesium substituted [15] and copper substituted [18] NiCuZn ferrites were prepared through the egg-white method. The thermogravimetry (TG), XRD, TEM and FT-IR characterization techniques proved the ferrite formation at relatively low calcination temperature. Improved magnetic properties were obtained due to magnesium substitution [15] and as a result of the utilized preparation method [18].

In the present work, we report an attempt on the structural and magnetic properties with the addition of nonmagnetic Cr^{3+} in NiCuZn ferrite prepared by egg-white method. In addition we aimed to produce low cost ferrite materials according to the desired application by easy and inexpensive synthesis technique. To the authors' knowledge, there are still no related reports so far, and some new results obtained may be helpful for the preparation of high-performance NiZnCu ferrites.

2. Experimental procedures

Egg-white method [15,18] is a simple, cheap, cost-effective, nontoxic and environmentally friend method. The use of egg-white simplifies the process and would provide another alternative process for the simple and economical synthesis of nano-ferrites. Egg-white protein is a natural matrix of poly amino acids (contain amino and carboxylic groups in their structure). Due to its solubility in water and its ability to associate with metal ions in solution, egg-white has been used as a binder cum gel for shaping material, particularly bulk and porous ceramics. When this precursor is ignited, nano-ferrite phases can be obtained at relatively lower temperatures than the other preparation methods.

Ferrite nanoparticles of nominal composition $Ni_{0.50}Cu_{0.25}Zn_{0.25}Fe_{2-x}Cr_xO_4$ where x varying from 0.0 to 1.0 were prepared by egg-white method. Nickel nitrate, copper nitrate, zinc nitrate, ferric nitrate and chromium nitrate, in their respective stoichiometry, were dissolved in 100 ml distilled water. Sixty milliliters of freshly extracted egg-white was dissolved in 40 ml distilled water and mixed thoroughly, at room temperature, with the nitrate mixture. After vigorous stirring for 30 min, the resultant sol–gel was dried at 80 °C until a dry precursor was obtained. The dried powder was grounded thoroughly and calcined in an electric muffle at 350 or 450 °C for 1 h or 550 °C for 2 h.

Differential scanning calorimetry–thermogravimetry–differential thermogravimetry (DSC–TG–DTG) were carried out, using Netzsch STA 409 thermal analyzer on precursors up to 600 °C at a heating rate of 5 °C min^{-1} in air.

The ferrite formation and crystallite size were determined from XRD measurements carried out on D8 Advance diffractometer (Bruker AXS, Germany) using CuKα radiation ($\lambda = 1.5406$ Å). Crystallite sizes were determined from the full width at half maximum (FWHM) of the most intense reflections using the Scherrer formula [19].

Fourier transform infrared spectroscopic analysis using KBr pellets was carried out using a Jasco model FT-IR 310 spectrophotometer.

The particle size was determined by transmission electron microscopy (TEM) using a Jeol 2010 transmission electron microscope with an accelerating voltage of 100 kV.

The magnetization measurements were done at room temperature up to a maximum external field; $H_m = 8$ kOe using Lakeshore Model 7404 Vibrating Sample Magnetometer (VSM).

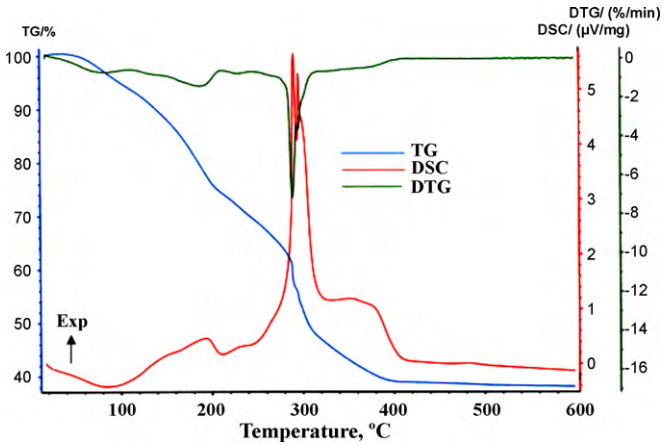

Fig. 1. DSC–TG–DTG curves in air of precursor with Cr content of 0.4. Heating rate = 5 °C min^{-1}.

3. Results and discussion

3.1. Thermal analysis studies

The minimum temperature for the complete decomposition process, which can be considered as the minimum temperature for the calcination process, can be estimated from the thermal behavior measurements of the dried precursors. Fig. 1 shows typical DSC–TG–DTG curves in air for the as-prepared egg-white precursor with Cr content of 0.4. The first weight loss before 100 °C can be attributed to the evaporation of the residual water. The following successive TG steps are attributed to the oxidative decomposition of the residual nitrate and organic matter. The weight of the precursor appears to be constant for temperatures above 350 °C.

The peaks in the DSC and DTG curves closely correspond to the weight loss observed on the TG trace. The endothermic DSC peak in the range of 35–140 °C is attributed to the dehydration of the precursor. The successive exothermic DSC peaks are attributed to the oxidative decomposition of the precursor.

3.2. Structural studies

X-ray diffraction of the as-prepared precursors exhibited completely amorphous patterns at all compositions. The samples calcined at the minimum calcination temperature estimated from thermal analysis measurements (350 °C) show the appearance of some crystallinity. The crystallinity is observed to increase by increasing the calcination temperature to 450 °C. Fig. 2 shows typical X-ray diffraction patterns for the as-prepared sample with Cr content of 0.6 and samples calcined at 350 and 450 °C.

The XRD patterns presented in Fig. 3 confirm that all the calcined samples at 550 °C are in the crystalline state with cubic spinel ferrite phases. No extra lines corresponding to any other phases can be detected. The peaks were indexed by comparing the interplanar distances with JCPDS data [20]. The values of lattice constants for different chromium concentrations were calculated by analyzing the XRD patterns [15].

Lattice parameters and crystallite sizes of the sintered ferrite specimens, evaluated by XRD analysis, are shown in Table 1 along with their theoretical density. There was a minor decrease in lattice parameter (a) with chromium substitution, which may be due to the smaller difference in the ionic radii of 6-fold-coordinated Cr^{3+} (0.63 Å) compared to that of 6-fold coordinated high spin Fe^{3+} (0.64 Å) [19]. With increasing chromium content, the crystallite size (D_x) was observed to decrease up to chromium content of 0.4 then gradually increase. The nearly constant X-ray density obtained for

Table 1
Lattice parameters, X-ray densities, average crystallite size, FT-IR spectral data and magnetic data of $Ni_{0.50}Cu_{0.25}Zn_{0.25}Fe_{2-x}Cr_xO_4$ system.

Parameters	$x=0.0$	$x=0.2$	$x=0.4$	$x=0.6$	$x=0.8$	$x=1.0$
Lattice parameter, a (Å)	8.396	8.377	8.370	8.360	8.355	8.350
X-ray density, D_x ($g\,cm^{-3}$)	5.33	5.34	5.34	5.34	5.33	5.33
Average crystallite size, D (nm)	25	21	15	17	19	22
Tetrahedral vibration, ν_1 (cm^{-1})	593	595	597	598	600	601
Octahedral vibration, ν_2 (cm^{-1})	402	409	412	417	420	423
Saturation magnetization, M_s ($emu\,g^{-1}$)	44.4	36.0	25.9	19.8	16.1	9.4
Magnetic moment, η_B (μB)	1.89	1.52	1.09	0.83	0.67	0.39
Remenant magnetization, M_r ($emu\,g^{-1}$)	7.9	5.7	3.7	3.4	2.5	1.2
Coercivity, H_c ($emu\,g^{-1}$)	52.1	32.0	28.8	48.9	66.9	92.88

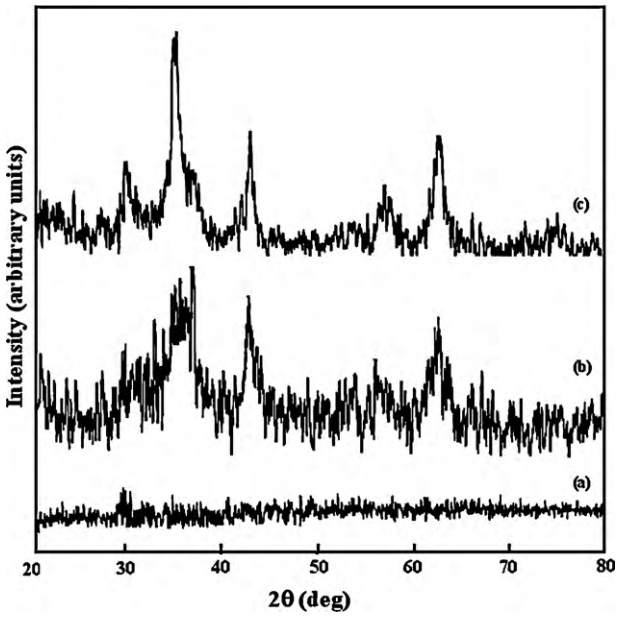

Fig. 2. XRD patterns of the precursor with Cr content of 0.6, calcined at different temperatures: (a) as-prepared precursor; (b) precursor calcined at 350 °C; (c) precursor calcined at 450 °C.

all compositions is expected since, the decrease in the molecular weight of the sample (attributed to the smaller atomic weight of the chromium compared with that of iron) is accompanied by a decrease in the lattice constant.

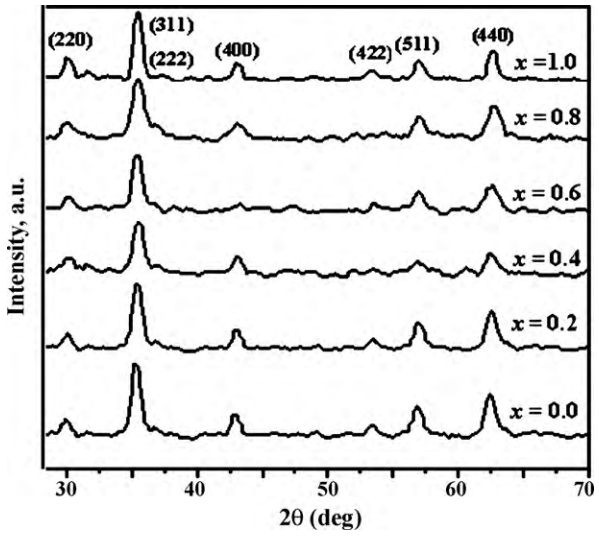

Fig. 3. Characteristic parts of XRD patterns of $Ni_{0.50}Cu_{0.25}Zn_{0.25}Fe_{2-x}Cr_xO_4$ system calcined at 550 °C.

FT-IR spectra of the ferrite nanoparticles calcined at 550 °C are presented in Fig. 4. Vibrations of ions in the crystal lattice are usually observed in the range of 1000–400 cm^{-1}. Two main broad metal–oxygen bands are observed in the FT-IR spectra of all spinels, and ferrites in particular. The highest one, ν_1, is generally observed around 600 cm^{-1}, and it corresponds to intrinsic stretching vibrations of the metal at the tetrahedral site, whereas the lowest band, ν_2, is usually observed around 400 cm^{-1}, is assigned to octahedral-metal stretching [21]. FT-IR spectral data of the present system are summarized in Table 1. From the table it is clear that, the band positions at frequency ν_1 is nearly constant with increasing Cr content. Meanwhile, it can be seen that the frequency ν_2 is gradually shifted to higher frequencies with increasing Cr ion concentration. Cr ions are well

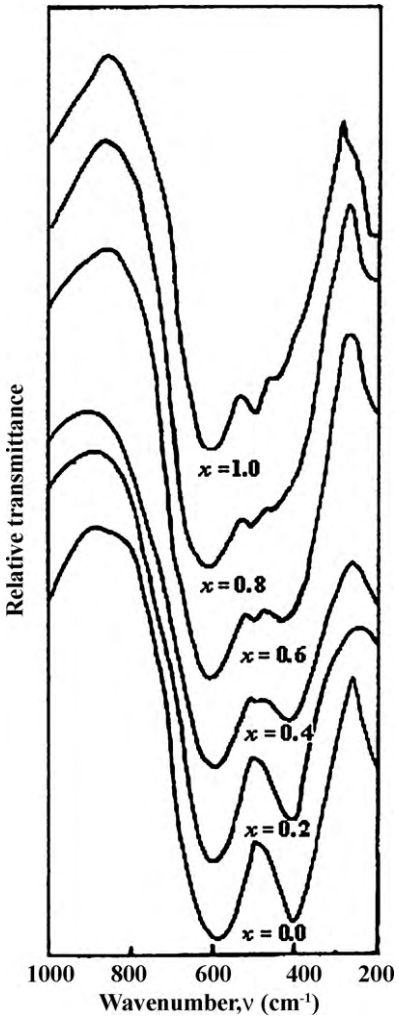

Fig. 4. FT-IR spectra of $Ni_{0.50}Cu_{0.25}Zn_{0.25}Fe_{2-x}Cr_xO_4$ system calcined at 550 °C.

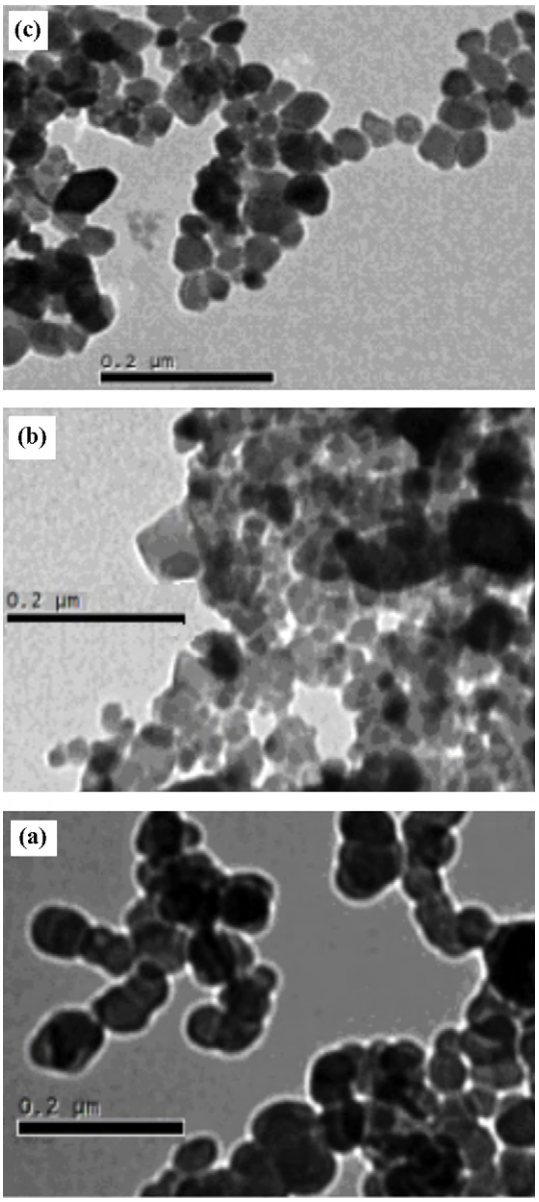

Fig. 5. TEM images at different Cr content: (a) $x = 0.0$; (b) $x = 0.6$; (c) $x = 1.0$.

known to occupy preferentially the octahedral sites. The shift in the band position, by increasing Cr content, may be due to the variation in the cation–oxygen bond length of the octahedral lattice of the spinel. The displacement of Fe^{3+} ions by smaller Cr^{3+} ions will results into a somewhat decrease in the metal–oxygen bond length and consequently increase the wave number of ν_2 band.

It is also observed that the intensity of octahedral band decreases with the addition of Cr and the difference between the intensities of the tetrahedral and octahedral bands becomes prominent. It is known that the intensity ratio is a function of the change of dipole moment with the internuclear distance ($d\mu/dr$). The electronic distribution of Fe–O bonds is greatly affected when a Cr^{3+} ion, with comparatively smaller radius and low atomic weight, is introduced in its neighborhood and this consequently affects its ($d\mu/dr$) [19,22,23].

The absorption bands corresponding to metal ions present in the octahedral site, show splitting into two bands with increasing Cr content. A similar behavior was also detected in similar ferrites systems [19,24]. The absence of the low frequency bands in our compounds suggests that the lattice vibrations responsible for these bands are very weak.

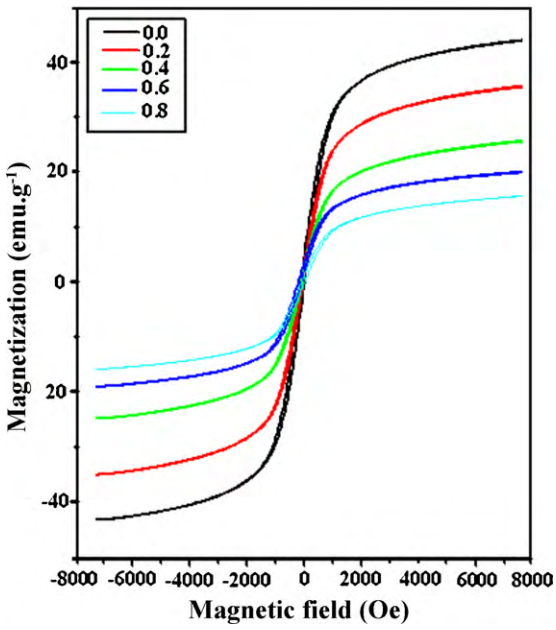

Fig. 6. Magnetic hysteresis loops for $Ni_{0.50}Cu_{0.25}Zn_{0.25}Fe_{2-x}Cr_xO_4$ system.

The morphologies and particle sizes of the samples with Cr content of 0.0, 0.6 and 1.0 calcined at 550 °C, are shown in Fig. 5. From the figure, it is clear that the particles are spherical in shape and are agglomerated to some extent. This agglomeration can be attributed to the magnetic dipole interactions arising between ferrite particles [25]. The estimated average particle sizes are around 28, 19 and 23 nm, respectively. This agrees well with that estimated using XRD measurements.

3.3. Magnetic studies

Room temperature magnetization curves of the samples calcined at 550 °C (Fig. 6) show that saturation has not been reached even in the maximum measured field of 8 kOe. The reason of this can be that the magnitude of the magnetic field required to reach saturation magnetization depends on the size of the particles [23,26–28]. From the figure it is also clear that, all compositions analyzed produced a narrow loops, with a behavior characteristic of soft magnetic materials (easy magnetization and demagnetization) [29].

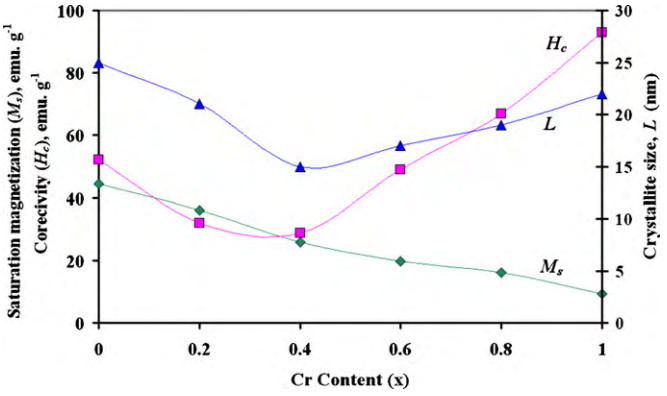

Fig. 7. Variation of the saturation magnetization, coercivity and the particle size with Cr content in $Ni_{0.50}Cu_{0.25}Zn_{0.25}Fe_{2-x}Cr_xO_4$ system.

The values of saturation magnetization (M_s), coercivity (H_c), remenant magnetization (M_r) and magnetic moment (η_B) are listed in Table 1. Fig. 7 plots the saturation magnetization (M_s), coercivity (H_c) and the particle size as a function of chromium content. It is clear that, the saturation magnetization linearly decreases with increasing chromium concentration whereas, the coercive field decreases up to chromium content of 0.4 then gradually increases.

According to Neel's sublattice theory [30], the net magnetic moments in ferromagnetic ferrite materials depend on the number of magnetic ions occupying the tetrahedral and octahedral sites. The Cr^{3+} ions with magnetic moment of 2.81 μB have a tendency to replace Fe^{3+} ions with magnetic moment 5 μB on the octahedral site causing a decrease of magnetic moment of this sublattice resulting in the decrease of the total magnetic moment and consequently, magnetization.

The H_c is known to be affected by several factors, most important of which is the particle size [31]. Fig. 6 shows that it exhibits the same behavior as that displayed by the particle size. Generally, H_c was found proportional to the particle size according to the linear fit to the data through many literatures [31,32].

4. Conclusions

A simple, cost-effective and environmentally friendly method using egg-white was utilized to prepare single phase Cr-substituted NiCuZn nanocrystalline ferrites. DSC–TG–DTG, XRD, FT-IR and TEM techniques were used to confirm the composition and structure of the spinel ferrite. Magnetic measurements showed that the nanoparticles did not attain saturation at room temperature even in the presence of relatively high magnetic field of 8 kOe. Saturation magnetization was found to decrease with Cr content while coercivity is proportionally changed with the particle size.

Acknowledgement

The authors are grateful to King Abdul Aziz University for providing financial support for this work.

References

[1] C. Venkataraju, G. Sathishkumar, K. Sivakumar, J. Magn. Magn. Mater. 322 (2010) 230.
[2] H. Su, H. Zhang, X. Tang, Z. Zhong, Y. Jing, Mater. Sci. Eng. B 162 (2009) 22.
[3] H. Su, H. Zhang, X. Tang, J. Magn. Magn. Mater. 302 (2006) 278.
[4] P.K. Roy, J. Bera, J. Magn. Magn. Mater. 298 (2006) 38.
[5] C. Miao, J. Zhou, X. Cui, X. Wang, Z. Yue, L. Li, Mater. Sci. Eng. B 127 (2006) 1.
[6] A. Pradeep, P. Priyadharsini, G. Chandrasekaran, J. Magn. Magn. Mater. 320 (2008) 2774.
[7] S.G. Doh, E.B. Kim, B.H. Lee, J.H. Oh, J. Magn. Magn. Mater. 272–276 (2004) 2238.
[8] B. Baruwati, R.K. Rana, S.V. Manorama, J. Appl. Phys. 101 (2007) 0143021.
[9] H. Yang, X. Zhang, W. Ao, G. Qiu, Mater. Res. Bull. 39 (2004) 833.
[10] X.D. Li, W.S. Yang, F. Li, D.G. Evans, X. Duan, J. Phys. Chem. Solids 67 (2006) 1286.
[11] M.M. Hessien, J. Magn. Magn. Mater. 320 (2004) 2800.
[12] L. Ai, J. Jiang, Curr. Appl. Phys. 10 (2010) 284.
[13] M.A. Gabal, Y.M. Al Angari, J. Magn. Magn. Mater. (2010), doi:10.1016/j.jmmm.2010.05.054.
[14] M.A. Gabal, S.A. Al-Thabaiti, E.H. El-Mossalamy, M. Mokhtar, Ceram. Int. 36 (2010) 1339.
[15] M.A. Gabal, J. Magn. Magn. Mater. 321 (2009) 3144.
[16] N. Chu, X. Wang, Y. Liu, H. Jin, Q. Wu, L. Li, Z. Wang, H. Ge, J. Alloys Compd. 470 (2009) 438.
[17] P.K. Roy, J. Bera, J. Magn. Magn. Mater. 321 (2009) 247.
[18] M.A. Gabal, Y.M. Al Angary, S.S. Al-Juaid, J. Alloys Compd. 492 (2010) 411.
[19] M.A. Gabal, Y.M.A. Angari, Mater. Chem. Phys. 118 (2009) 153.
[20] International Center for Diffraction Data, JCPDS, PDF2 Data Base, Swarthmore, PA, USA, 1996.
[21] R.D. Waldron, Phys. Rev. 99 (1955) 1727.
[22] A.M. El-Sayed, Ceram. Int. 28 (2002) 651.
[23] P. Priyadharsini, A. Pradeep, P. Sambasiva Rao, G. Chandrasekaran, Mater. Chem. Phys. 116 (2009) 207.
[24] F.A. Lopez, A. Lopez-Delgado, J.L. Martın de Vidales, E. Vila, J. Alloys Compd. 265 (1998) 291.
[25] L. Li, C. Xiang, X. Liang, B. Hao, Synth. Met. 160 (2010) 28.
[26] B. Martinez, X. Obradors, Ll. Balcells, A. Rouanet, C. Monty, Phys. Rev. Lett. 80 (1998) 181.
[27] S. Dey, J. Ghose, Mater. Res. Bull. 38 (2003) 1653.
[28] M. Mozaffari, S. Manouchehri, M.H. Yousefi, J. Amighian, J. Magn. Magn. Mater. 322 (2010) 383.
[29] A.C.F.M. Costa, V.J. Silva, H.S. Ferreira, A.A. Costa, D.R. Cornejo, R.H.G.A. Kiminami, L. Gama, J. Alloys Compd. 483 (2009) 655.
[30] S. Chikazumi, Physics of Ferromagnetism, 2nd ed., Oxford Science Publications, 1997.
[31] H. Li, H. Wu, G. Xiao, Powder Technol. 198 (2010) 157.
[32] Y. Liu, S. He, D. Bao, X. Ren, Chin. J. Magn. Mater. Devices 34 (3) (2003) 28.